Weighted Sum Rate Maximization for RIS-mounted UAV-aided Cell-Free ISAC Systems

Shanza Shakoor, *Student Member, IEEE,* Nguyen-Son Vo, Quang Nhat Le, *Member, IEEE,* Berk Canberk, *Senior Member, IEEE,* Chao-Kai Wen, *Fellow, IEEE,* Hyundong Shin, *Fellow, IEEE,* and Trung Q. Duong, *Fellow, IEEE*

***Abstract*—This paper considers the cell-free integrated sensing and communication (CF-ISAC) networks utilizing reconfigurable intelligent surface (RIS)-mounted uncrewed aerial vehicles (UAVs). We aim to maximize the sum of weighted sum rate within the whole ISAC period by jointly optimizing access points (APs)' transmit beamformings, RISs' phase shifts, user-RIS association, and UAVs' locations. To deal with a highly complex non-convex optimization problem, we propose an alternating optimization solutions by decomposing the original problem into three subproblems. In particular, for optimizing APs' transmit beamformings, RISs' phase shifts, and user-RIS association, we convert the log-sum problem into a quadratically constrained quadratic programming problem using the Lagrangian dual principle and multi-ratio fractional programming. For optimizing UAVs' locations, the successive convex approximation technique is used to transform it into a convex problem. Simulation results highlight the considerable performance advantage of the proposed network compared to benchmark schemes employing fixed RISs, without RIS-mounted UAVs (URISs), and collocated network with URISs.**

***Index Terms*—Cell-free (CF), integrated sensing and communication (ISAC), joint optimization, reconfigurable intelligent surface (RIS), uncrewed aerial vehicle (UAV).**

S. Shakoor and Q. N. Le are with the Dept. of Electrical and Computer Engineering, Memorial University, St. John's, NL A1B 3X9, Canada (e-mail: {sshakoor, qnle}@mun.ca).

N.-S. Vo is with the Institute of Fundamental and Applied Sciences, Duy Tan University, Ho Chi Minh City, 70000, Vietnam, and also with the Faculty of Electrical-Electronic Engineering, Duy Tan University, Da Nang, 50000, Vietnam (e-mail: vonguyenson@duytan.edu.vn).

B. Canberk is with the School of Engineering and Built Environment, Edinburgh Napier University, Edinburgh EH10 5DT, UK, (e-mail: b.canberk@napier.ac.uk).

C.-K. Wen is with the Institute of Communications Engineering, National Sun Yat-sen University, Kaohsiung 80424, Taiwan (e-mail: chaokai.wen@mail.nsysu.edu.tw).

H. Shin is with the Department of Electronics and Information Convergence Engineering, Kyung Hee University, 1732 Deogyeong-daero, Giheung-gu, Yongin-si, Gyeonggi-do 17104, Republic of Korea (e-mail: hshin@khu.ac.kr).

T. Q. Duong is with the Faculty of Engineering and Applied Science, Memorial University, St. John's, NL A1C 5S7, Canada, and with the School of Electronics, Electrical Engineering and Computer Science, Queen's University Belfast, Belfast, U.K, and also with the Department of Electronic Engineering, Kyung Hee University, Yongin-si, Gyeonggi-do 17104, South Korea (e-mail: tduong@mun.ca).

This work was supported in part by the Canada Excellence Research Chair (CERC) Program CERC-2022-00109 and in part by the Natural Sciences and Engineering Research Council of Canada (NSERC) Discovery Grant Program RGPIN-2025-04941. The work of B. Canberk is supported in part by The Scientific and Technological Research Council of Turkey (TUBITAK) Frontier R&D Laboratories Support Program for BTS Advanced AI Hub: BTS Autonomous Networks and Data Innovation Lab Project 5239903. The work of C.-K. Wen was supported in part by the National Science and Technology Council of Taiwan through grants NSTC 114-2218-E-110-006, and by the Sixth Generation Communication and Sensing Research Center, which is funded by the Higher Education SPROUT Project of the Ministry of Education (MOE) of Taiwan. The work of H. Shin was supported in part by National Research Foundation of Korea (NRF) grant funded by the Korean government (MSIT) (RS-2025-00556064).

This paper has been accepted in part for presentation at 7th Computers, Communications and IT Applications Conference (ComComAp 2025), Madrid, Spain, December 2025.

Corresponding authors are Trung Q. Duong and Hyundong Shin.

I. Introduction

In recent years, the rapid advancement of wireless technologies and the increasing demand for seamless connectivity have driven continuous innovation in wireless network systems. With the development of sixth-generation (6G) networks, there are growing expectations for extremely fast data speeds, nearly zero delay in connections, and smart networks that can automatically adjust. These future networks will need to support many new technologies, such as self-driving cars, smart cities, drones, healthcare systems, and more [1], [2].

To address these demands, integrated sensing and communication (ISAC) has emerged as a promising approach that combines communication and sensing functionalities into a unified platform [3], [4]. By enabling the concurrent execution of wireless transmission and environmental perception over the same frequency spectrum and hardware infrastructure, ISAC significantly improves spectrum efficiency, reduces latency, lowers hardware cost, and enhances situational awareness, making it indispensable for 6G applications, such as intelligent transportation systems, smart cities, and uncrewed systems.

However, deploying ISAC in real-world environments, especially large and dynamic ones, is quite challenging. Traditional cellular networks, which depend on centralized base stations, often face signal coverage problems and low sensing performance in areas where obstacles block the line-of-sight (LoS) signals, like cities with tall buildings, forests, or hilly regions [5]–[7]. These limitations have led to the development of cell-free ISAC (CF-ISAC) networks, which remove fixed cell boundaries and use a large number of access points (APs) spread across the area to jointly serve users and perform sensing tasks [8], [9]. This decentralized structure enhances signal strength, reduces interference, and improves location accuracy. However, it also introduces new challenges, including coordinating beamforming, managing interference, and allocating network resources.

To further enhance communication reliability and sensing precision, a promising advancement in CF-ISAC is the integration of reconfigurable intelligent surfaces (RISs). RISs consist of passive and programmable meta-surfaces that can dynamically manipulate electromagnetic waves, thereby improving signal strength and coverage in challenging environments [10]–[13]. Furthermore, RIS can help improve both

communication and sensing by redirecting signals toward users and targets in challenging locations, reducing interference, and making better use of the wireless spectrum [14]. However, when RISs are installed in fixed positions, their functionality is limited by the surrounding environment and infrastructure. For instance, if a user moves behind a building, a stationary RIS may no longer provide effective support.

To solve this issue, uncrewed aerial vehicles (UAVs) mounted RIS (URIS) systems have been proposed. These airborne RISs can move freely, adjusting their position in real-time to optimize both communication and sensing wherever they are most needed [15]. This makes it possible to perform 3D beamforming by optimizing both the UAV's position and the RIS configuration, which leads to better network coverage, stronger communication links, and more accurate sensing [15], [16].

However, combining UAV with RIS also makes the system more complex. It becomes necessary to jointly optimize several things at once like the UAV's flight path, the phase shifts of the RIS, and the way communication signals are sent and received. These optimization tasks become even harder when the number of users and network demands increase. Another important part of CF-ISAC systems with URIS is RIS-user association deciding which user should be served by which RIS. If the system connects a user to a distant URIS, the signal might be weak. So, the system must carefully decide which URIS should help which users in each situation. A good RIS-user association strategy balances communication quality and sensing accuracy by efficiently assigning users to URISs based on their positions, signal conditions, and network needs [17], [18].

Given these technical challenges and practical needs, this paper focuses on designing a joint optimization framework for CF-ISAC networks assisted by URISs. The main goal is to improve both communication and sensing performance by jointly optimizing UAV's trajectories, RIS's phase shifts, beamforming strategies, and RIS-user associations in a dynamic and distributed environment.

TABLE I
VARIABLE DEFINITION

Notation	Description
L	Number of APs
F	Number of SRs
K	Number of Users
R	Number of RISs
M	Number of antennas at each AP and SR
N	Number of reflecting elements at each RIS
T	Total number of time slots
t	Time slot index
$\mathbf{q}_{t,r}$	2D position vector of URIS r at time slot t
$\mathbf{w}_{t,l,k}$	Beamforming vector of AP l at time slot t for user k
$\mathbf{w}_{t,l,0}$	Beamforming vector of AP l at time slot t for sensing target
$\mathbf{W}_l$	Aggregate beamforming matrix of AP l
$\mathbf{\Theta}_{t,r}$	Diagonal phase-shift matrix of RIS r at time slot t
$\mathbf{d}_{t,lr}$	Distance between AP l and RIS r at time slot t
$\mathbf{d}_{t,r0}$	Distance between RIS r and target at time slot t
$\mathbf{d}_{t,rk}$	Distance between RIS and user k at time slot t
$\mathbf{G}_{t,l,r}$	Channel from AP l to RIS r at time slot t
$\mathbf{g}_{t,l,k}$	Direct channel vector from AP l to user k at time slot t
$\mathbf{g}_{t,r,k}$	Channel from RIS r to user k at time slot t
$\mathbf{g}_{t,r,s}$	Channel from RIS r to target at time slot t
$\mathbf{g}_{t,f}$	Channel from target to SR f at time slot t
$\mathbf{G}_{t,s}$	Cascade channel AP-RIS-target-SR at time slot t
$u_{t,k,r}$	Association between RIS r and user k at time slot t
$\gamma_{t,k}$	SINR received at user k
$\gamma_{t,s}$	Joint sensing SNR
Υ_t	Weighted sum rate of all users at time slot t

A. Related Work

ISAC has become a promising approach to solve spectrum scarcity by allowing both sensing and communication to use the same time and frequency resources [19], [20]. While early research primarily centered on centralized or single-cell architectures, recent efforts have extended ISAC principles to more scalable and distributed frameworks. One such example is CF multi-input multi-output (MIMO), where many distributed APs serve users cooperatively. This architecture improves network coverage and provides better user experience, making it suitable for joint sensing and communication tasks [21]–[24].

In [25], the authors proposed a multi-static CF-ISAC system using a maximum a posteriori (MAP)-based detector and a power control algorithm to improve sensing performance while meeting communication needs. Similarly, the authors in [26] studied how to allocate power in distributed multi-antenna systems for a single user, either using one base station or in a cell-free setup. They used regularized zero-forcing beamforming, where the sensing beam was placed in the null-space of the communication channel. However, this method did not include any extra optimization steps to improve system performance. Furthermore, joint sensing-communication (JSC) beamforming was studied in [23] using a max-min fairness approach. The authors compared communication-prioritized and sensing-prioritized beamforming and showed that optimized beamforming can improve overall system performance. The results show that their joint design approach offers a communication signal-to-interference-plus-noise-ratio (SINR) nearly matching that of the communication-prioritized scheme, while also maintaining a sensing signal-to-noise ratio (SNR) comparable to the sensing-prioritized method.

To improve flexibility and signal quality, several works

have added RIS to CF-ISAC systems. For example, [6] proposed a RIS-assisted full-duplex CF-ISAC setup where APs' beamforming, RIS's phase shifts, and power allocation were jointly optimized using fractional programming (FP) and majorization-minimization (MM) algorithms. In [27], the authors focused on securing CF-ISAC systems from eavesdroppers by designing joint communication and sensing beamformers using semidefinite relaxation (SDR). The authors in [13] investigated a RIS-assisted ISAC system and proposed a joint design of transmit beamforming and RIS's phase shifts to maximize communication SNR while ensuring sensing accuracy using a Cramér-Rao bound (CRB) constraint. The authors formulated a non-convex optimization problem and solved it using penalty dual decomposition and successive convex approximation (SCA). The results demonstrate an effective trade-off between sensing precision and communication performance. Additionally, the authors in [28] studied a CF-ISAC system assisted by multiple RISs and focused on maximizing the minimum SINR across users while optimizing APs' beamforming and RISs' phase shifts. They proposed an alternating optimization (AO) method to jointly improve communication and sensing performance. Results showed that their approach effectively boosts both user fairness and sensing quality. However, in all of the above-discussed studies, the RIS was placed in a fixed location, so it couldn't adapt to changing network demands.

To address dynamic environments, some recent studies have introduced URIS to CF-ISAC networks. For instance, [29] used deep reinforcement learning to optimize the UAV's path along with beamforming and RIS control in a ISAC system with single antenna users. In contrast, [30] tackled a multi-user setup by optimizing UAV's location, active beamforming at BSs, and passive beamforming at the RIS using SCA and FP, showing improvements in rate and coverage. Furthermore, the work in [31] proposed a URIS-assisted ISAC system that jointly optimizes the UAV's position, transmit beamforming, and RIS's phase shifts to enhance communication secrecy and sensing accuracy. The authors used techniques like particle swarm optimization (PSO), SDR, and MM to solve the non-convex problem efficiently. Results show improved secrecy rates and sensing performance, making the approach suitable for secure ISAC applications.

It is important to note that these URIS-based studies operate in conventional ISAC architectures with a single BS or centralized controller. In contrast, none of these works consider the distributed CF-ISAC framework, where multiple APs and SRs jointly serve users and the sensing target under CPU coordination. Therefore, the CF-ISAC architecture with multiple URISs studied in this paper differs fundamentally in system assumptions and design challenges. Furthermore, one crucial aspect, i.e., RIS-user association, remains underexplored. [17] and [32] have focused on RIS-user association and beamforming using optimization techniques. However, these were mainly applied to traditional cellular systems and did not support sensing features, UAV's constraints, or dynamic RIS configuration. Despite improved efficiency, the method did not incorporate sensing or UAV's mobility.

B. Motivation and Contributions

The integration of ISAC into CF architectures, enhanced by the flexibility of URIS, has opened new directions in wireless system design. Existing CF-ISAC researches have made substantial progress in enhancing spectral efficiency, joint beamforming, and secure communication. However, several critical challenges remain unaddressed. Most existing studies assume static RIS placements, limiting the system's ability to dynamically adapt to user distribution and channel variations. Additionally, RIS-user association is typically fixed or ignored, which restricts the system from fully leveraging RISs in multi-user setups. UAV-mounted RIS, offering mobility and coverage flexibility, has emerged as a promising enhancement, but prior work often considers simplified or single user models. Furthermore, UAV's energy constraints and multi-static sensing capabilities are rarely incorporated into joint optimization frameworks.

These limitations are clearly summarized in Table II, which compares the scope of existing works against key dimensions: ISAC integration, CF architecture, URIS, RIS-user association, and UAV's energy constraints. As shown, most existing studies cover only a subset of these aspects, often assuming static RIS deployments or neglecting joint optimization involving RIS-user mapping and UAV's energy constraints.

Motivated by these gaps, we propose a comprehensive CF-ISAC framework that leverages URISs to provide flexible signal reflection, improved coverage, and energy-efficient operation in multi-user environments. To the best of our knowledge, this is the first work to jointly optimize APs' beamforming, RISs' phase shifts, RIS-user association, and UAVs' placement, under both UAVs' energy constraints and multi-static sensing considerations, with the objective of maximizing the weighted sum rate in a multi-user CF-ISAC system.

Our main contributions are summarized as follows:

- We propose an URIS-assisted CF-ISAC system that maximizes the achievable weighted sum rates within the whole ISAC period while satisfying radar sensing constraints.
- We design a joint optimization framework to maximize the weighted sum rate within the whole ISAC period by optimizing APs' beamforming, RISs' phase shifts, RIS-user association, and UAVs' positioning. This is done while also considering radar sensing requirements and the UAVs' energy limitations. The problem is challenging due to the coupling among the involved variables.
- We incorporate multi-static radar sensing into the CF-ISAC system by using URISs to assist in signal reflection for sensing.
- To solve the optimization problem, we develop an efficient AO framework that divides the considered problem into three subproblems including APs' beamforming, RISs' phase shift design with RIS-user association, and UAVs' location optimization. First, we transform the objective function with logarithmic terms by applying the Lagrangian dual method, which helps simplify the non-convex expressions. Then, to handle the non-convex multi-ratio fractional terms, we use the multi-dimensional complex quadratic transform (MCQT) for optimizing

TABLE II
COMPARISON OF RELATED WORKS AND OUR KEY CONTRIBUTIONS

Ref	ISAC	CF	URIS	RIS-user association	UAV's energy constraints
[6]	✓	✓	✗	✗	✗
[17]	✗	✓	✗	✓	✗
[23]	✓	✓	✗	✗	✗
[25]	✓	✓	✗	✗	✗
[28]	✓	✓	✗	✗	✗
[29]	✓	✗	✓	✗	✓
[30]	✗	✓	✓	✗	✗
[32]	✗	✗	✗	✓	✗
[33]	✓	✓	✗	✗	✗
[34]	✓	✗	✓	✗	✓
our paper	✓	✓	✓	✓	✓

APs' beamforming and RISs' phase shifts, which reformulates them into a more tractable form as a quadratically constrained quadratic programming (QCQP) problem. To address the user-RIS association subproblem, we introduce a penalty-based method to manage the non-convex and discrete nature of the user-to-RIS assignment. Next, for UAV placement, we apply the SCA technique. These subproblems are then solved iteratively in an alternating manner until convergence is achieved.

- Our simulation results show that using URISs improve weighted sum rate, sensing performance, and network coverage. The proposed method works better than other baseline schemes, proving its effectiveness.

The remainder of this paper is organized as follows. Section II describes the system model. Section III outlines the problem formulation, which involves the joint design of APs' beamforming, RIS's phase shifts and RIS-user association, and URISs' location. Section IV presents the proposed solution framework to maximize the weighted sum rate through joint optimization of all involved variables. Section V provides simulation results and performance evaluation. Finally, Section VI concludes the paper and discusses future research directions.

C. Notation

We use vectors in bold lowercase (e.g., $\mathbf{w}$) and matrices in bold uppercase (e.g., $\mathbf{W}$). The transpose, conjugate, and conjugate transpose (Hermitian transpose) of $\mathbf{W}$ are $\mathbf{W}^T$, $\mathbf{W}^\dagger$, and $\mathbf{W}^H$, respectively. The absolute value and Euclidean norm of $\mathbf{W}$ are $|\mathbf{W}|$ and $\|\mathbf{W}\|$. The space of $M \times 1$ complex-valued vectors is $\mathbb{C}^{M\times 1}$, and $M \times N$ complex-valued matrices are denoted by $\mathbb{C}^{M\times N}$. The Hermitian transpose of $\mathbf{W}$ is $\mathbf{W}^H$, and $\text{diag}(\boldsymbol{\psi})$ is a diagonal matrix with entries from $\boldsymbol{\psi}$. The real part of an expression is extracted using $\Re\{\cdot\}$, and $\mathbf{I}_N$ represents the $N \times N$ identity matrix.

II. SYSTEM MODEL

As illustrated in Fig. 1, we consider a system comprising multiple URISs to enhance the communication and sensing quality within a CF-ISAC network. The system includes a set

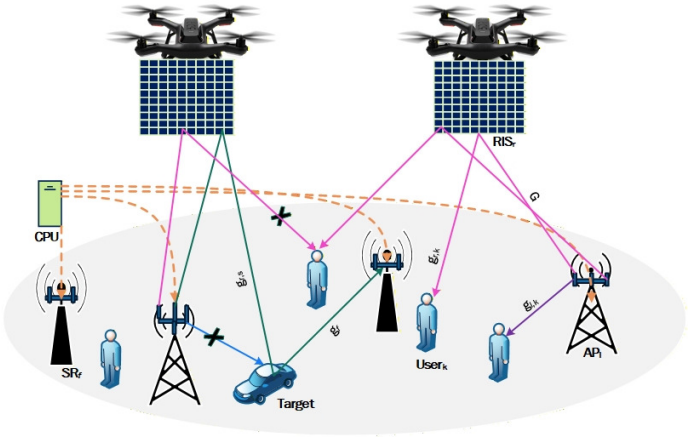

Fig. 1. The system model of CF-ISAC network with URISs.

of $\mathcal{L} = \{1, \ldots, L\}$ APs, $\mathcal{F} = \{1, \ldots, F\}$ sensing receivers (SRs), $\mathcal{R} = \{1, \ldots, R\}$ URISs, $\mathcal{K} = \{1, \ldots, K\}$ users, and a single sensing target. Each AP and each SR is equipped with M antennas arranged as a uniform linear array (ULA), used for transmitting communication and radar signals at the APs and receiving radar echoes at the SRs. Each RIS consists of $\mathcal{N} = \{1, \ldots, N\}$ reflecting elements to improve the communication and sensing from the APs to single-antenna users and the target, respectively. All APs and SRs are connected to a central server via high-speed wired links, while the URISs communicate wirelessly with the central server, forming a unified and high-performance network infrastructure.

The UAV and RIS act as a single entity for simplicity and the impact of the RIS's size and weight on the solution is neglected [30]. The URISs are only allowed to fly within a defined horizontal area E, and each URIS $r \in \mathcal{R}$ operates at a fixed altitude, based on safety regulations and stability constraints [29], [34]. The ISAC operation, with a total duration T_0, is partitioned into T uniform time slots, each with a fixed duration ϱ, such that $T_0 = T\varrho$. The r-th URIS location at time slot t is expressed as $\mathbf{q}_{t,r} = [x_{t,r}, y_{t,r}]$, i.e., $\mathbf{q}_{t,r} \in E$. Furthermore, each URIS starts from an individual initial location $\mathbf{q}_{r,0} = [x_{r,0}, y_{r,0}]$. To ensure flight safety and

operational constraints, the UAV is restricted to the designated area $\mathcal{X} \times \mathcal{Y}$, throughout its mission, formalized as

$$\mathbf{q}_{t,r} \in \mathcal{X} \times \mathcal{Y}, \quad \forall t \in \{1, 2, \ldots, T\}, \quad \forall r \in \mathcal{R}. \tag{1}$$

Moreover, the UAV's mobility is subject to a maximum allowable velocity $\upsilon_{\max}$, yielding the constraint

$$\|\mathbf{q}_{t,r} - \mathbf{q}_{t,r-1}\| \leq \varrho \upsilon_{\max}, \quad \forall t = \{2, \ldots, T\}, \quad \forall r \in \mathcal{R}. \tag{2}$$

Following common simplifying assumptions in multi-UAV planning [35], [36], we consider straight-line URIS trajectories from their initial positions to the optimized locations and assume that they operate in a controlled airspace with sufficiently separated configurations (e.g., through altitude planning), so that inter-URIS collisions do not occur during the translation.

The propulsion energy consumed by the r-th URIS is mainly influenced by its velocity, acceleration, and flight duration. The instantaneous propulsion energy expenditure at time slot t, for r-th URIS, is given by

$$\mathcal{E}_{t,r}^{\text{URIS}} = \left[P_0 \left(1 + \frac{3\upsilon_{t,r}^2}{U_{\text{tip}}^2} \right) + P_1 \left(\sqrt{1 + \frac{\upsilon_t^4}{4\upsilon_0^4}} - \frac{\upsilon_{t,r}^2}{2\upsilon_0^2} \right)^{\frac{1}{2}} + \wp \upsilon_{t,r}^3 \right] \varrho, \tag{3}$$

$$\upsilon_{t,r} = \frac{||\mathbf{q}_{t,r} - \mathbf{q}_{t,r-1}||}{\varrho}, \tag{4}$$

where $\upsilon_{t,r}$ denotes the r-th URIS's velocity at time slot t. $P_0, P_1, U_{\text{tip}}, \upsilon_0$, and $\wp$ are system dependent constants determined by the aerodynamics and propulsion characteristics of the URIS platform. The standard numerical values for these parameters are summarized in Table III [29], [34]. Furthermore, the UAV's limited flight time is implicitly enforced through the total propulsion-energy constraint [37].

TABLE III
STANDARD PARAMETER VALUES FOR (3)

Parameter	Description	Value
P_0	Blade profile power	80 W
U_{tip}	Blade tip speed	120 m/s
υ_0	Mean rotor induced velocity	4 m/s
$\upsilon_{\max}$	Maximum allowable velocity	20 m/s
P_1	Induced power coefficient	31.43 W
$\wp$	Fuselage drag coefficient	0.0046 kg/m

The spatial location of r-th URIS at time slot t can be denoted as $\mathbf{q}_{t,r}^R = (x_{t,r}^R, y_{t,r}^R)^T$. The l-th AP, the k-th user, and the target are positioned at $\boldsymbol{\chi}_l^L = (x_l^L, y_l^L)^T$, $\boldsymbol{\chi}_k^K = (x_k^K, y_k^K)^T$, and $\boldsymbol{\chi}_0 = (x_0, y_0)^T$, respectively. The height of k-th user, target, l-th APs and r-th URIS is denoted as h_k, h_o, h_l, and h_r, respectively. The distance between the r-th URIS and l-th AP, target, and k-th user is respectively denoted by

$$d_{t,lr} = \sqrt{\|\mathbf{q}_{t,r}^R - \boldsymbol{\chi}_l^L\|^2 + |h_r - h_l|^2}, \tag{5}$$

$$d_{t,r0} = \sqrt{\|\mathbf{q}_{t,r}^R - \boldsymbol{\chi}_0\|^2 + |h_r - h_0|^2}, \tag{6}$$

$$d_{t,rk} = \sqrt{\|\mathbf{q}_{t,r}^R - \boldsymbol{\chi}_k^K\|^2 + |h_r - h_k|^2}. \tag{7}$$

A. Transmission Model

The complex baseband signal at time slot t transmitted by l-th AP is represented as

$$\mathbf{x}_{t,l} = \sum_{k \in \mathcal{K}} \mathbf{w}_{t,l,k} s_{t,k} + \mathbf{w}_{t,l,0} s_{t,0}, \tag{8}$$

where $\mathbf{w}_{t,l,k} \in \mathbb{C}^{M \times 1}$ and $\mathbf{w}_{t,l,0} \in \mathbb{C}^{M \times 1}$ denote the beamforming vectors for transmitting data to k-th user and sensing stream to target, respectively, with $s_{t,k}$ and $s_{t,0}$ representing the associated k-th user's data and sensing stream.

B. Channel Model

The AP-user link consists of both LoS and URIS-assisted non-LoS paths, while the AP-target direct LoS link is assumed to be blocked due to environmental obstructions [33]. Therefore, only the URIS-assisted AP-to-target links are considered. Additionally, a direct LoS link is assumed between the target and the SRs, ensuring reliable signal reception for radar sensing tasks. Furthermore, we assume perfect CSI for all links, which can be obtained using effective channel estimation methods [38]. The channel gains at time slot t between the l-th AP and r-th RIS, r-th RIS and k-th user, r-th RIS and target, l-th AP and k-th user, f-th SR and target are denoted by $\mathbf{G}_{t,l,r} \in \mathbb{C}^{N \times M}$, $\mathbf{g}_{t,r,k} \in \mathbb{C}^{N \times 1}$, $\mathbf{g}_{t,r,s} \in \mathbb{C}^{N \times 1}$, $\mathbf{g}_{t,l,k} \in \mathbb{C}^{M \times 1}$, and $\mathbf{g}_{t,f} \in \mathbb{C}^{M \times 1}$, respectively, which are shown as

$$\mathbf{G}_{t,l,r} = \sqrt{\alpha d_{t,lr}^{-2}} \left(\sqrt{\frac{\beta}{\beta+1}} \mathbf{G}_{t,lr}^{\text{LoS}} + \sqrt{\frac{1}{\beta+1}} \mathbf{G}_{t,lr}^{\text{NLoS}} \right), \tag{9}$$

$$\mathbf{g}_{t,r,k} = \sqrt{\alpha d_{t,rk}^{-2}} \left(\sqrt{\frac{\beta}{\beta+1}} \mathbf{g}_{t,rk}^{\text{LoS}} + \sqrt{\frac{1}{\beta+1}} \mathbf{g}_{t,rk}^{\text{NLoS}} \right), \tag{10}$$

$$\mathbf{g}_{t,r,s} = \sqrt{\alpha d_{t,rs}^{-2}} \left(\sqrt{\frac{\beta}{\beta+1}} \mathbf{g}_{t,rs}^{\text{LoS}} + \sqrt{\frac{1}{\beta+1}} \mathbf{g}_{t,rs}^{\text{NLoS}} \right), \tag{11}$$

$$\begin{aligned} \mathbf{g}_{t,l,k} &= \sqrt{\alpha d_{t,lk}^{-2}} \left(\sqrt{\frac{\beta}{\beta+1}} \mathbf{g}_{t,lk}^{\text{LoS}} + \sqrt{\frac{1}{\beta+1}} \mathbf{g}_{t,lk}^{\text{NLoS}} \right), \\ &= \sqrt{\alpha d_{t,lk}^{-2}} \mathbf{g}_{t,lk}^{\text{LoS}}, \end{aligned} \tag{12}$$

$$\begin{aligned} \mathbf{g}_{t,f} &= \sqrt{\alpha d_{t,fs}^{-2}} \left(\sqrt{\frac{\beta}{\beta+1}} \mathbf{g}_{t,fs}^{\text{LoS}} + \sqrt{\frac{1}{\beta+1}} \mathbf{g}_{t,fs}^{\text{NLoS}} \right), \\ &= \sqrt{\alpha d_{t,fs}^{-2}} \mathbf{g}_{t,fs}^{\text{LoS}}, \end{aligned} \tag{13}$$

where α and β represent the path loss per unit distance and the Rician factor, respectively. $\mathbf{G}_{t,lr}^{\text{NLoS}}$, $\mathbf{g}_{t,rk}^{\text{NLoS}}$, and $\mathbf{g}_{t,rs}^{\text{NLoS}}$ represent the NLoS channel components, which follow the

Gaussian distribution. The LoS component of the $\mathbf{G}_{t,l,r}$ channel is given by

$$\mathbf{G}_{t,lr}^{\mathrm{LoS}} = \mathbf{a}_r^H(\theta_{t,r,l}, \phi_{t,r,l})\mathbf{a}_l(\theta_{t,l,r}, \phi_{t,l,r}), \tag{14}$$

where $\theta_{t,l,r}$ and $\phi_{t,l,r}$ represent the elevation and azimuth angles, respectively. Since each AP and each URIS are equipped with the ULA of size $M = M_x \times M_y$ and $N = N_x \times N_y$, respectively, where M_x and M_y represent the number of antenna elements at each AP along the x-axis and y-axis, while N_x and N_y denote the numbers of reflecting elements at each URIS along the corresponding axes. The array response vector is defined as

$$\begin{aligned}\mathbf{a}_l(\theta_{t,l,r}, \phi_{t,l,r}) = \left[1, \ldots, e^{-j2\pi \frac{d}{\lambda}(M_x-1)\sin(\theta_{t,l,r})\sin(\phi_{t,l,r})}\right] \\ \otimes \left[1, \ldots, e^{-j2\pi \frac{d}{\lambda}(M_y-1)\cos(\theta_{t,l,r})}\right],\end{aligned}$$

$$\begin{aligned}\mathbf{a}_r(\theta_{t,r,l}, \phi_{t,r,l}) = \left[1, \ldots, e^{j2\pi \frac{d}{\lambda}(N_x-1)\sin(\theta_{t,r,l})\cos(\phi_{t,r,l})}\right] \\ \otimes \left[1, \ldots, e^{j2\pi \frac{d}{\lambda}(N_y-1)\sin(\theta_{t,r,l})\sin(\phi_{t,r,l})}\right],\end{aligned}$$

where the spatial parameters are calculated as

$$\sin(\theta_{t,l,r})\sin(\phi_{t,l,r}) = \frac{y_{t,r}^R - y_l^L}{d_{t,lr}}, \tag{15}$$

$$\cos(\theta_{t,l,r}) = \frac{h_r - h_l}{d_{t,lr}}, \tag{16}$$

$$\sin(\theta_{t,r,l})\cos(\phi_{t,r,l}) = \frac{x_l^L - x_{t,r}^R}{d_{t,lr}}, \tag{17}$$

$$\sin(\theta_{t,r,l})\sin(\phi_{t,r,l}) = \frac{y_l^L - y_{t,r}^R}{d_{t,lr}}. \tag{18}$$

C. Communication Model

For each user, the signal transmitted from the APs can propagate through two distinct paths: the direct AP-to-user link and the indirect AP-to-URIS-to-user link, where the RIS enhances connectivity by reflecting the signal towards the user. To model the association between users and RISs, let $u_{t,k,r} \in \{0, 1\}$ indicate whether k-th user is associated with r-th RIS or not. The association vector for k-th user, representing its connection to all RISs, is given by

$$\mathbf{u}_{t,k} = [u_{t,k,1}, \ldots, u_{t,k,R}]^T. \tag{19}$$

For all users and RISs, the association matrix is represented as

$$\mathcal{U}_t = [\mathbf{u}_{t,1}, \ldots, \mathbf{u}_{t,K}]^T \in \mathbb{R}^{K \times R}. \tag{20}$$

Therefore, the signal received by the k-th user at time slot t is expressed as

$$\mathbf{y}_{t,k} = \sum_{l \in \mathcal{L}} \sum_{r \in \mathcal{R}} (\mathbf{g}_{t,l,k}^H + u_{t,k,r}\mathbf{g}_{t,r,k}^H \mathbf{\Theta}_{t,r}\mathbf{G}_{t,l,r})\mathbf{x}_{t,l} + n_{t,k}, \tag{21}$$

where $n_{t,k} \sim \mathcal{CN}(0, \sigma_{t,k}^2)$ denotes the additive white Gaussian noise (AWGN) with variance $\sigma_{t,k}^2$ at the k-th user. The phase shift matrix of the r-th RIS, represented by

$$\begin{aligned}\mathbf{\Theta}_{t,r} &= \mathrm{diag}(e^{j\theta_{t,r,1}}, \ldots, e^{j\theta_{t,r,N}}) \\ &= \mathrm{diag}\left(\psi_{t,r,1}, \ldots, \psi_{t,r,N}\right),\end{aligned} \tag{22}$$

defines the phase shift matrix of the r-th RIS, where $\theta_{t,r,n}$ denotes the phase shift of the n-th element at time slot t. It is assumed that these phase shift values can be continuously tuned within the interval $[0, 2\pi)$. The received SINR at time slot t at the k-th user can expressed as

$$\gamma_{t,k} = \frac{|\mathbf{g}_{t,k}^H \mathbf{w}_{t,k}|^2}{\sum\limits_{j \in \bar{\mathcal{K}} \setminus k} |\mathbf{g}_{t,k}^H \mathbf{w}_{t,j}|^2 + \sigma_{t,k}^2}, \tag{23}$$

where

$$\hat{\mathbf{g}}_{t,l,k}^H = (\mathbf{g}_{t,l,k}^H + u_{t,k,r}\mathbf{g}_{t,r,k}^H \mathbf{\Theta}_{t,r}\mathbf{G}_{t,l,r}), \tag{24}$$

$$\bar{\mathcal{K}} = \mathcal{K} \cup \{0\}, \tag{25}$$

$$\mathbf{g}_{t,k} = \left[\hat{\mathbf{g}}_{t,1,k}^H \ldots, \hat{\mathbf{g}}_{t,L,k}^H\right]^H, \tag{26}$$

$$\mathbf{w}_t \triangleq \{\mathbf{w}_{t,l,0}, \mathbf{w}_{t,l,k}\}_{l \in \mathcal{L}, k \in \mathcal{K}}, \tag{27}$$

$$\mathbf{w}_{t,0} = \left[\mathbf{w}_{t,1,0}^H, \ldots, \mathbf{w}_{t,L,0}^H\right]^H, \tag{28}$$

$$\mathbf{w}_{t,k} = [\mathbf{w}_{t,1,k}^H, \ldots, \mathbf{w}_{t,L,k}^H]^H. \tag{29}$$

The weighted sum rate of all users at time slot t can be expressed as

$$\Upsilon_t = \sum_{k \in \mathcal{K}} \varpi_{t,k} \log_2(1 + \gamma_{t,k}), \tag{30}$$

where $\varpi_{t,k}$ denotes the communication weight of k-th user at time slot t.

D. Sensing Model

We consider a multi-static sensing configuration, illustrated in Fig. 2, where the transmitters and receivers are deployed at separate locations. In this setup, L APs are responsible for transmitting the sensing signals, while F SRs collaboratively receive these signals to detect the target. The CPU then collects and processes the signals from all F SRs to perform target detection [28], [39]. The signal received at the f-th SR at time slot t can be expressed as

$$\boldsymbol{y}_{f,t} = \sum_{l \in \mathcal{L}} \sum_{r \in \mathcal{R}} \kappa_{f,l}\mathbf{G}_{t,s}\boldsymbol{x}_l + \mathbf{n}_{f,t}, \tag{31}$$

where the sensing channel between transmit AP l and SR f is defined as [33], [40]

$$\mathbf{G}_{t,s} = \mathbf{g}_{t,f}(\mathbf{G}_{t,l,r}^H \mathbf{\Theta}_{t,r}\mathbf{g}_{t,r,s})^H, \tag{32}$$

and the radar cross section (RCS) for the sensing path between transmit AP l and SR f is denoted by $\kappa_{f,l}$. According to the Swerling-I model, the RCS is assumed to remain constant throughout the transmission period and is modeled as a complex Gaussian random variable, $\kappa_{f,l} \sim \mathcal{CN}(0, \sigma_{f,l}^2)$. We assume that all $\kappa_{f,l}$ values are known in advance, and that the RCS values for different transmitter-receiver pairs

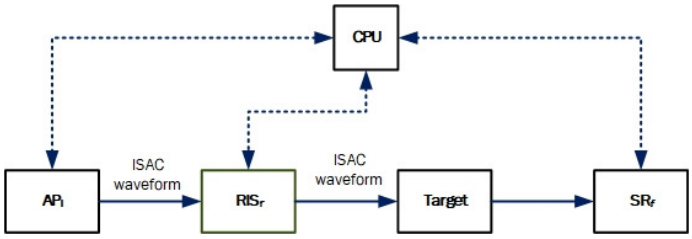

Fig. 2. RIS-aided multi-static sensing.

are statistically independent. This assumption is commonly adopted in multi-static sensing models [41], where the RCS associated with a given target class is treated as a known parameter. The receiver noise at the f-th SR is denoted by

$$\mathbf{n}_{f,t} \sim \mathcal{CN}(\mathbf{0}, \sigma_{t,s}^2 \mathbf{I}_M) \in \mathbb{C}^{M\times 1}. \tag{33}$$

Hence, the joint sensing SNR at the CPU can be derived by jointly processing the signals from all SRs and is given by [33]

$$\gamma_{t,s} = \frac{\sum\limits_{f\in\mathcal{F}}\sum\limits_{l\in\mathcal{L}} \kappa_{f,l}||\mathbf{G}_{t,s}\mathbf{W}_l||^2}{F\sigma_{t,s}^2}, \tag{34}$$

where

$$\mathbf{W}_l = [\mathbf{w}_{l,0}, \mathbf{w}_{l,1}, \ldots, \mathbf{w}_{l,K}] \in \mathbb{C}^{M\times(K+1)}, \tag{35}$$

concatenates the beamforming vectors of all users and the sensing target.

III. Problem Formulation

Our objective is to maximize the sum of weighted sum rates within the whole ISAC period, through the joint optimization of beamforming $\mathbf{w}$, phase shifts Θ, UAVs' locations $\mathbf{q}$, and RIS-user association $\mathcal{U}$. Let us define

$$\mathbf{w} \triangleq \{\mathbf{w}_t\}_{t\in T}, \tag{36}$$

$$\mathbf{\Theta} \triangleq \{\mathbf{\Theta}_r\}_{r\in\mathcal{R}}, \tag{37}$$

$$\mathbf{q} \triangleq \{\mathbf{q}_r^R\}_{r\in\mathcal{R}}, \tag{38}$$

$$\mathcal{U} \triangleq \{\mathcal{U}_t\}_{t\in T}. \tag{39}$$

Therefore, the optimization problem can be formulated as

$$\max_{\substack{\mathbf{w}_t,\mathbf{\Theta}_t,\mathbf{q}_t,\\ \mathcal{U}_t,\forall t}} \sum_{t\in T} \quad \Upsilon_t \tag{40a}$$

s.t.

$$\gamma_{t,s} \geq \gamma_{th}^{sens}, \forall t, \tag{40b}$$

$$\|\mathbf{w}_{t,l,0}\|^2 + \sum_{k\in\mathcal{K}} \|\mathbf{w}_{t,l,k}\|^2 \leq P_{t,l}^{\max}, \forall l \in \mathcal{L}, \forall t, \tag{40c}$$

$$|\psi_{t,r,n}| = 1, \forall r \in \mathcal{R}, \forall n \in \mathcal{N}, \forall t, \tag{40d}$$

$$\sum_{r\in\mathcal{R}} u_{t,k,r} \leq R_{connect}, \forall k \in \mathcal{K}, \forall t, \tag{40e}$$

$$u_{t,k,r} \in \{0,1\}, \forall k \in \mathcal{K}, \forall r \in \mathcal{R}, \forall t, \tag{40f}$$

$$\mathbf{q}_{t,r}^R \in E, \forall r \in \mathcal{R}, \forall t, \tag{40g}$$

$$\sum_{t\in T} \mathcal{E}_{t,r}^{\text{URIS}}(\mathbf{q}_{t,r}) \leq \mathcal{E}^{\max}, \forall t, \forall r \in \mathcal{R}, \tag{40h}$$

$$\frac{||\mathbf{q}_{t,r} - \mathbf{q}_{t,r-1}||}{\varrho} \leq \upsilon_{max}, \forall t, \forall r \in \mathcal{R}. \tag{40i}$$

Constraints (40b) and (40c) represent the minimum sensing SNR requirement for the target and the maximum transmit power for the l-th AP, respectively. Constraint (40e) illustrates the number of URIS with which k-th user can be paired is limited to $R_{connect}$. Finally, constraints (40h) and (40i) represent the URIS's energy limitation and the maximum allowable flying speeds, respectively. Problem (40) is non-convex because of the non-concave objective function (40a) and non-convex constraints (40b), (40d), (40f), and (40h).

IV. Proposed Solution

A. Transformation of Objective Function

To simplify the objective function (40a), we use the FP method to convert the objective function into a more favorable polynomial expression. As derived in [13], [42], we introduce an auxiliary variable $\mathbf{b}_t = [b_{t,1}, b_{t,2}\ldots, b_{t,K}]^T$ to separate the ratio term $\gamma_{t,k}$ in (30) from the logarithmic function via the Lagrangian dual reformulation. This transforms (40a) into a solvable polynomial form at time slot t, expressed as

$$\sum_{k\in\mathcal{K}} \varpi_{t,k}\log_2(1+b_{t,k}) - \sum_{k\in\mathcal{K}} \varpi_{t,k} b_{t,k} + \sum_{k\in\mathcal{K}} \frac{\varpi_{t,k}(1+b_{t,k})\gamma_{t,k}}{1+\gamma_{t,k}}, \tag{41}$$

where the optimal value of $b_{t,k}$ at time slot t can be obtained by computing the first-order partial derivative of equation (41) with respect to $b_{t,k}$ and setting it equal to zero. When this optimal value is found, the objective function in (40a) becomes equivalent to (41). The value of $b_{t,k}$ at optimality is therefore determined by

$$b_{t,k}^* = \gamma_{t,k}. \tag{42}$$

Nevertheless, the final term in (41) remains a complex non-convex fraction. To simplify the solution process, we apply a quadratic transformation [13], [42] to convert it into a more

tractable form, which is shown as follows:

$$2\sqrt{\varpi_{t,k}(1+b_{t,k})}\Re\{\delta_{t,k}^{*}\mathbf{g}_{t,k}^{H}\mathbf{w}_{t,k}\}-|\delta_{t,k}|^{2}\left(\sum_{j\in\bar{\mathcal{K}}\setminus k}|\mathbf{g}_{t,k}^{H}\mathbf{w}_{t,j}|+\sigma_{t,k}^{2}\right), \tag{43}$$

where the optimal value of the relaxation variable $\delta_{t,k}$ is determined by

$$\delta_{t,k}^{*}=\frac{\sqrt{\varpi_{t,k}(1+b_{t,k})}\mathbf{g}_{t,k}^{H}\mathbf{w}_{t,k}}{\sum\limits_{j\in\bar{\mathcal{K}}\setminus k}|\mathbf{g}_{t,k}^{H}\mathbf{w}_{t,j}|+\sigma_{t,k}^{2}}. \tag{44}$$

After determining the auxiliary variables $b_{t,k}$ and $\delta_{t,k}$, and applying the corresponding transformations in (41) and (43), the objective function (40a) can be expressed in terms of $\mathbf{w}_t$ and $\mathbf{\Theta}_t$ as

$$\begin{aligned}f(\mathbf{w}_t,\mathbf{\Theta}_t,\mathbf{q}_{t,r},b_{t,k},\delta_{t,k})=&\sum_{k\in\mathcal{K}}2\sqrt{\varpi_{t,k}(1+b_{t,k})}\Re\{\delta_{t,k}^{*}\mathbf{g}_{t,k}^{H}\mathbf{w}_{t,k}\}\\&-\sum_{k\in\mathcal{K}}|\delta_{t,k}|^{2}\left(\sum_{j\in\bar{\mathcal{K}}\setminus k}|\mathbf{g}_{t,k}^{H}\mathbf{w}_{t,j}|+\sigma_{t,k}^{2}\right).\end{aligned} \tag{45}$$

B. Beamforming Optimization

With fixed $\mathbf{\Theta}_t,\mathbf{q}_t,b_{t,k},\delta_{t,k},\mathcal{U}_t$, the transmit beamforming optimization problem is reduced to

$$\max_{\mathbf{w}_t,\forall t}\quad\sum_{t\in T}\sum_{k\in\mathcal{K}}2\sqrt{\varpi_{t,k}(1+b_{t,k})}\Re\{\delta_{t,k}^{*}\mathbf{g}_{t,k}^{H}\mathbf{w}_{t,k}\} \tag{46a}$$

$$-\sum_{t\in T}\sum_{k\in\mathcal{K}}|\delta_{t,k}|^{2}\left(\sum_{j\in\bar{\mathcal{K}}\setminus k}|\mathbf{g}_{t,k}^{H}\mathbf{w}_{t,j}|+\sigma_{t,k}^{2}\right)$$

s.t.

$$(40b),(40c), \tag{46b}$$

where numerator term of $\gamma_{t,s}$ in the non-convex constraint (40b) is convexified by employing the following inequality

$$||\boldsymbol{\tau}||^{2}\geq 2\Re\{(\boldsymbol{\tau}^{(t)})^{H}\boldsymbol{\tau}\}-||\boldsymbol{\tau}^{(t)}||^{2}, \tag{47}$$

where $\boldsymbol{\tau}=\mathbf{G}_{t,s}\mathbf{W}_l$. This technique effectively convexifies the numerator term of $\gamma_{t,s}$. As a result, (40b) is rewritten as

$$\frac{\sum\limits_{f\in\mathcal{F}}\sum\limits_{l\in\mathcal{L}}\kappa_{f,l}\left(2\Re\{(\boldsymbol{\tau}^{(t)})^{H}\boldsymbol{\tau}\}-||\boldsymbol{\tau}^{(t)}||^{2}\right)}{F\sigma_{t,s}^{2}}\geq\gamma_{th}^{sens}. \tag{48}$$

C. Phase Shift and User-RIS Association Optimization

With fixed $\mathbf{w}_t,\mathbf{q}_t,b_{t,k},\delta_{t,k}$, the URISs' phase shifts and user-RIS association optimization problem can be formulated as

$$\max_{\Theta_t,\mathcal{U}_t,\forall t}\quad\sum_{t\in T}\sum_{k\in\mathcal{K}}2\sqrt{\varpi_{t,k}(1+b_{t,k})}\Re\{\delta_{t,k}^{\dagger}\boldsymbol{\psi}_t^{H}\mathbf{g}_{t,k,k}\} \tag{49a}$$

$$-\sum_{t\in T}\sum_{k\in\mathcal{K}}|\delta_{t,k}|^{2}\left(\sum_{j\in\bar{\mathcal{K}}\setminus k}\boldsymbol{\psi}_t^{H}\mathbf{g}_{t,k,j}\mathbf{g}_{t,k,j}^{H}\boldsymbol{\psi}_t+\sigma_{t,k}^{2}\right)$$

s.t.

$$(40b),(40d),(40e),(40f), \tag{49b}$$

where

$$\delta_{t,k}^{\dagger}=\frac{\sqrt{\varpi_{t,k}(1+b_{t,k})}\boldsymbol{\psi}_t^{H}\mathbf{g}_{t,k,j}}{\sum\limits_{j\in\bar{\mathcal{K}}\setminus k}\boldsymbol{\psi}_t^{H}\mathbf{g}_{t,k,j}\mathbf{g}_{t,k,j}^{H}\boldsymbol{\psi}_t+\sigma_{t,k}^{2}}, \tag{50}$$

$$\begin{aligned}\mathbf{g}_{t,k,j}^{H}\mathbf{w}_{t,k,k}&=\sum_{l\in\mathcal{L}}\sum_{r\in\mathcal{R}}\left(\mathbf{g}_{t,l,k}+\mathbf{u}_{t,k}^{T}\mathbf{g}_{t,r,k}^{H}\mathbf{\Theta}_{t,r}\mathbf{G}_{t,l,r}\right)\mathbf{w}_{t,l,j}\\&=\boldsymbol{\psi}_t^{H}\mathbf{g}_{t,k,j},\\\mathbf{g}_{t,k,j}&=\sum_{l\in\mathcal{L}}\sum_{r\in\mathcal{R}}\left(\mathrm{diag}(\mathbf{g}_{t,r,k}^{H})\mathbf{G}_{t,l,r}\right)\mathbf{w}_{t,l,j},\\\mathbf{g}_{t,k,j}^{H}&=\varrho+\mathbf{u}_{t,k}^{T}\boldsymbol{\zeta}_{t,k,j},\end{aligned} \tag{51}$$

where

$$\zeta_{t,k,j,r}=\sum_{l\in\mathcal{L}}\mathbf{g}_{t,r,k}^{H}\mathbf{\Theta}_{t,r}\mathbf{G}_{t,l,r}\mathbf{w}_{t,l,j}, \tag{52}$$

$$\boldsymbol{\zeta}_{t,k,j}=\left[\zeta_{t,k,j,1},\ldots,\zeta_{t,k,j,R}\right]^{T}, \tag{53}$$

$$\varrho=\sum_{l\in\mathcal{L}}\mathbf{g}_{t,l,k}\mathbf{w}_{t,l,j}. \tag{54}$$

Similarly,

$$\mathbf{g}_{t,s}\mathbf{w}_{t,l}=\sum_{l\in\mathcal{L}}\sum_{r\in\mathcal{R}}\left[\mathbf{g}_{t,f}(\mathbf{g}_{t,r,s}^{H}\mathbf{\Theta}_{t,r}\mathbf{G}_{t,l,r})\right]\mathbf{w}_{t,l}, \tag{55}$$

where

$$\mathbf{g}_{t,s}=\sum_{l\in\mathcal{L}}\sum_{r\in\mathcal{R}}\mathbf{g}_{t,f}\left[\boldsymbol{\psi}_t^{H}\mathrm{diag}(\mathbf{g}_{t,r,s}^{H})\mathbf{G}_{t,l,r}\right]. \tag{56}$$

Hence, (40b) can be approximated as

$$\sum_{t\in T}\kappa_{f,l}\Re\left\{\mathbf{w}_l^{H}\mathbf{g}_{t,s}^{H}\mathbf{g}_{t,s}\mathbf{w}_l\right\}-F\sigma_{t,s}^{2}\geq\gamma_{th}^{sens}. \tag{57}$$

Next, for the binary association variable indicating the user-RIS matching $u_{t,k,r}$, we first relax (40f) into a continuous variable. Let us define

$$\Xi(\mathbf{u}_t)=\sum_{r\in R}\sum_{k\in K}u_{t,r,k}, \tag{58}$$

$$\Pi(\mathbf{u}_t)=\sum_{r\in R}\sum_{k\in K}(u_{t,r,k})^{2}. \tag{59}$$

Then, we impose the following constraints [17]

$$\Xi(\mathbf{u}_t)-\Pi(\mathbf{u}_t)\leq 0,\forall t,\forall r,\forall k, \tag{60}$$

$$0\leq u_{t,r,k}\leq 1,\forall t,\forall r,\forall k. \tag{61}$$

Note that (60) represents a difference of convex (DC) programming relaxation constraint. The lower bound of $\Pi(\mathbf{u}_t)$

is derived as

$$\Pi(\mathbf{u}_t) \geq \Pi(\mathbf{u}_t^{(\varsigma)}) + \nabla_{u_t}\Pi(\mathbf{u}_t^{(\varsigma)})(\mathbf{u}_t - \mathbf{u}_t^{(\varsigma)}) \triangleq \Pi^{(\varsigma)}(\mathbf{u}_t), \tag{62}$$

$$\Xi(u_t) - \Pi^{(\varsigma)}(\mathbf{u}_t) \leq 0, \tag{63}$$

where at the ς-th iteration, $\Pi(\mathbf{u}_t^{(\varsigma)})$ represents the current value, and the gradient term is computed as

$$\nabla_{u_t}\Pi(\mathbf{u}_t^{(\varsigma)})(\mathbf{u}_t - \mathbf{u}_t^{(\varsigma)}) = \sum_{k\in\mathcal{K}}\sum_{r\in\mathcal{R}} 2(u_{t,r,k}^{(\varsigma)})(u_{t,r,k} - u_{t,r,k}^{(\varsigma)}). \tag{64}$$

By incorporating the constraint (63) as a penalty term in the objective function and introducing the slack variable $\wp_{t,k}^{(\varsigma)}$, we effectively address all non-convex terms in the association problem, and the convex approximation of problem (49) is formulated as

$$\max_{\substack{\boldsymbol{\Theta}_t,\mathbf{u}_t,\\ \wp_t,\forall t}} \quad \sum_{t\in T}\left(\sum_{k\in\mathcal{K}} 2\sqrt{\varpi_{t,k}(1+b_{t,k})}\Re\{\delta_{t,k}^{\dagger}\boldsymbol{\psi}_t^H\mathbf{g}_{t,k,k}\} \right. \tag{65a}$$

$$\left. - \sum_{k\in\mathcal{K}}|\delta_{t,k}|^2\left(\sum_{j\in\bar{\mathcal{K}}\setminus k}\boldsymbol{\psi}_t^H\mathbf{g}_{t,k,j}\mathbf{g}_{t,k,j}^H\boldsymbol{\psi}_t + \sigma_{t,k}^2\right) - \vartheta_t^{(\varsigma)}\wp_{t,k}^{(\varsigma)}\right)$$

s.t.

$$|\psi_{t,r,n}| \leq 1, \forall r\in\mathcal{R}, \forall n\in\mathcal{N}, \forall t, \tag{65b}$$

$$\sum_{r\in\mathcal{R}} u_{t,k,r} \leq R_{connect} + \wp_{t,k}^{(\varsigma)}, \quad \forall t, \forall k\in\mathcal{K}, \tag{65c}$$

$$(57), (63), \tag{65d}$$

where

$$\wp_{t,k}^{(\varsigma)} = (\Xi(u_t) - \Pi^{(\varsigma)}(u_t)), \tag{66}$$

which can be updated by

$$\wp_{t,k}^{(\varsigma)} = \max\left(0, \sum_{r=1}^{R} u_{t,k,r}^{(\varsigma)} - R_{\text{connect}}\right), \tag{67}$$

to permit violations. A penalty weight $\vartheta^{(\varsigma)}$ is applied to enforce $\wp_{t,k}^{(\varsigma)} \to 0$, ensuring that constraint (40e) is ultimately satisfied.

D. UAVs' Location Optimization

This section focuses on optimizing the location of the UAVs by decoupling the variables of the UAV for a streamlined process. With fixed $\boldsymbol{\Theta}_t, \mathbf{w}_t, b_{t,k}, \delta_{t,k}, \mathcal{U}_t$, we reformulate the channel equations as follows:

$$\begin{aligned}&(\mathbf{g}_{t,l,k}^H + u_{t,k,r}\mathbf{g}_{t,r,k}^H\boldsymbol{\Theta}_{t,r}\mathbf{G}_{t,l,r})\mathbf{w}_{t,l,j} \\ &= \sqrt{d_{t,lr}^{-2}d_{t,rk}^{-2}}(\mathbf{g}_{t,l,k}^H + u_{t,k,r}\hat{\mathbf{g}}_{t,r,k}^H\boldsymbol{\Theta}_{t,r}\hat{\mathbf{G}}_{t,l,r})\mathbf{w}_{t,l,j},\end{aligned} \tag{68}$$

where

$$\hat{\mathbf{G}}_{t,l,r} = \sqrt{\alpha}\left(\sqrt{\frac{\beta}{\beta+1}}\mathbf{G}_{t,lr}^{\text{LoS}} + \sqrt{\frac{1}{\beta+1}}\mathbf{G}_{t,lr}^{\text{NLoS}}\right), \tag{69}$$

$$\hat{\mathbf{g}}_{t,r,k} = \sqrt{\alpha}\left(\sqrt{\frac{\beta}{\beta+1}}\mathbf{g}_{t,rk}^{\text{LoS}} + \sqrt{\frac{1}{\beta+1}}\mathbf{g}_{t,rk}^{\text{NLoS}}\right). \tag{70}$$

Let us define

$$S_{t,l,k,j} = (\mathbf{g}_{t,l,k}^H + u_{t,k,r}\hat{\mathbf{g}}_{t,r,k}^H\boldsymbol{\Theta}_{t,r}\hat{\mathbf{G}}_{t,l,r})\mathbf{w}_{t,l,j}, \tag{71}$$

Then, we simplify

$$(\mathbf{g}_{t,l,k}^H + u_{t,k,r}\mathbf{g}_{t,r,k}^H\boldsymbol{\Theta}_{t,r}\mathbf{G}_{t,l,r})\mathbf{w}_{t,l,j} = \sqrt{d_{t,lr}^{-2}d_{t,rk}^{-2}}S_{t,l,k,j}. \tag{72}$$

The AP-RIS and user-RIS links depend on URIS's location, making optimization problem complex. To manage this, we adopt a local area optimization approach, restricting RIS movement within a small threshold to maintain a near-constant channel model. To maximize the weighted transmission rate, we define the optimization problem as follows:

$$\max_{\mathbf{q}_t,\forall t}\sum_{t\in T}\sum_{k\in\mathcal{K}}\varpi_{t,k}\tilde{\Upsilon}_{t,k}$$

s.t.

$$\mathbf{q}_{t,r} \in E, \tag{73a}$$

$$(40\text{h}), (40\text{i}). \tag{73b}$$

The rate function $\tilde{\Upsilon}_{t,k}$ is given by

$$\begin{aligned}\tilde{\Upsilon}_{t,k} = &\log_2\left(\sum_{l\in L}\sum_{j\in\mathcal{K}}\frac{S_{t,l,k,j}S_{t,l,k,j}^H}{d_{t,lr}^2d_{t,rk}^2} + \sigma_{t,k}^2\right) \\ &- \log_2\left(\sum_{l\in L}\sum_{j\in\bar{\mathcal{K}}\setminus k}\frac{S_{t,l,k,j}S_{t,l,k,j}^H}{d_{t,lr}^2d_{t,rk}^2} + \sigma_{t,k}^2\right).\end{aligned}$$

However, $\tilde{\Upsilon}_{t,k}$ is highly nonlinear, which complicates direct optimization. To address this, we introduce relaxation variables $X_{t,l,k}$ and $Y_{t,l,k}$, and reformulate $\tilde{\Upsilon}_{t,k}$ as a concave function as follows:

$$\begin{aligned}\tilde{\Upsilon}_{t,k} \geq \Upsilon_{t,k}^* = &\log_2\left(\sum_{l\in L}\sum_{j\in\mathcal{K}}\frac{S_{t,l,k,j}S_{t,l,k,j}^H}{X_{t,l,k}} + \sigma_{t,k}^2\right) \\ &- \frac{1}{\ln(2)}\sum_{l\in L}\sum_{j\in\mathcal{K}}\frac{S_{t,l,k,j}S_{t,l,k,j}^H(X_{t,l,k} - X_{t,l,k}^{(\varsigma)})}{(X_{t,l,k}^{(\varsigma)})^2} \\ &\times\left(\sum_{l\in L}\sum_{j\in\mathcal{K}}\frac{S_{t,l,k,j}S_{t,l,k,j}^H}{X_{t,l,k}} + \sigma_{t,k}^2\right)^{-1} \\ &- \log_2\left(\sum_{l\in L}\sum_{j\in\bar{\mathcal{K}}\setminus k}\frac{S_{t,l,k,j}S_{t,l,k,j}^H}{Y_{t,l,k}} + \sigma_{t,k}^2\right).\end{aligned} \tag{74}$$

For convexity, the constraint $X_{t,l,k} \geq d_{t,rk}^2d_{t,lr}^2$ must hold.

By using the SCA method, we approximate

$$\begin{aligned} d_{t,rk}^2 d_{t,lr}^2 \leq & \frac{1}{2}\left[(d_{t,rk}^2+d_{t,lr}^2)^2-(d_{t,rk}^{(\varsigma)})^4\right] \\ & -2(d_{t,rk}^{(\varsigma)})^2(\mathbf{q}_{t,r}-\boldsymbol{\chi}_k^K)^T(\mathbf{q}_{t,r}-\mathbf{q}_{t,r}^{(\varsigma)}) \\ & -2(d_{t,rk}^{(\varsigma)})^2(\mathbf{q}_{t,r}-\boldsymbol{\chi}_l^L)^T(\mathbf{q}_{t,r}-\mathbf{q}_{t,r}^{(\varsigma)}) \\ & =\Im_1(t,l,k). \end{aligned} \tag{75}$$

Thus, by leveraging SCA, we transform the problem into a convex optimization framework, ensuring an efficient solution. To ensure a lower bound on $\tilde{\Upsilon}_{t,k}$, the relaxation variable $Y_{t,l,k}$ must satisfy:

$$Y_{t,l,k} \leq d_{t,rk}^2 d_{t,lr}^2. \tag{76}$$

Since $d_{t,rk}^2 d_{t,lr}^2$ is a product of two convex terms, its upper approximation is formulated as

$$\begin{aligned} d_{t,rk}^2 d_{t,lr}^2 \geq & \frac{1}{2}\left[\left(d_{t,rk}^{(\varsigma)2}+d_{t,lr}^{(\varsigma)2}\right)^2-\left(d_{t,rk}^{(\varsigma)4}+d_{t,lr}^{(\varsigma)4}\right)\right] \quad (77a) \\ & +2\left[(d_{t,rk}^{(\varsigma)2}+d_{t,lr}^{(\varsigma)2})(\mathbf{q}_{t,r}^{(\varsigma)}-\boldsymbol{\chi}_k^K)^T(\mathbf{q}_{t,r}-\mathbf{q}_{t,r}^{(\varsigma)})\right] \\ & +2\left[(d_{t,rk}^{(\varsigma)2}+d_{t,lr}^{(\varsigma)2})(\mathbf{q}_{t,r}^{(\varsigma)}-\boldsymbol{\chi}_l^L)^T(\mathbf{q}_{t,r}-\mathbf{q}_{t,r}^{(\varsigma)})\right] \\ & =\Im_2(t,l,k). \end{aligned}$$

When $\Im_2(t,l,k) \geq Y_{t,l,k}$, the constraint $Y_{t,l,k} \leq d_{t,rk}^2 d_{t,lr}^2$ holds, ensuring convexity. Standard convex optimization methods, such as the primal-dual interior-point algorithm, are then applied to solve the problem.

Next, to address the nonconvexity of constraint (40h), we adopt a similar approach as in [43], [44], by introducing a per URIS slack variable $\{\mu_{t,r} \geq 0, \forall t, \forall r\}$, defined as

$$\mu_{t,r}^2 = \sqrt{1+\frac{\upsilon_{t,r}^4}{4\upsilon_0^4}}-\frac{\upsilon_{t,r}^2}{2\upsilon_0^2}, \tag{78}$$

which is equivalent to

$$\frac{1}{\mu_{t,r}^2} = \mu_{t,r}^2+\frac{\upsilon_{t,r}^2}{\upsilon_0}, \tag{79}$$

where the term $\frac{1}{\mu_{t,r}^2}$ is convex with respect to $\mu_{t,r}$, while the expression $\mu_{t,r}^2+\frac{\upsilon_{t,r}^2}{\upsilon_0}$ is jointly convex with respect to both $\{\mathbf{q}_{t,r}, \mu_{t,r}\}$. Thus, at given local points $\mathbf{q}_{t,r}^{(\varsigma)}$ and $\mu_{t,r}^{(\varsigma)}$, we approximate

$$\begin{aligned} \frac{1}{\mu_{t,r}^2} \leq & (\mu_{t,r}^{(\varsigma)})^2+\frac{(\upsilon_{t,r}^{(\varsigma)})^2}{\upsilon_0}+2\mu_{t,r}^{(\varsigma)}(\mu_{t,r}-\mu_{t,r}^{(\varsigma)}) \\ & +\frac{2\upsilon_{t,r}^{(\varsigma)}}{\upsilon_0}(\upsilon_{t,r}-\upsilon_{t,r}^{(\varsigma)})), \forall t, \forall r. \end{aligned} \tag{80}$$

As a result, the term $P_1\left(\sqrt{1+\frac{\upsilon_{t,r}^4}{4\upsilon_0^4}}-\frac{\upsilon_{t,r}^2}{2\upsilon_0^2}\right)^{\frac{1}{2}}\varrho$ in constraint (40h) can be approximated by the linear term $P_1\mu_{t,r}\varrho$. Consequently, the constraint (40h) can be reformulated as

$$\sum_{t\in T}\sum_{r\in\mathcal{R}}\left[P_0\left(1+\frac{3\upsilon_{t,r}^2}{U_{\text{tip}}^2}\right)\varrho+P_1\mu_{t,r}\varrho+\wp_{t,r}\upsilon_{t,r}^3\varrho\right] \leq \mathcal{E}^{\max}. \tag{81}$$

The convex approximation of problem (73) is given by

$$\max_{\mathbf{q}_{t,r},\forall t,\forall r} \quad \sum_{t\in T}\sum_{k\in\mathcal{K}}\Upsilon_{t,k}^* \tag{82a}$$

s.t.

$$\mathbf{q}_{t,r} \in E, \tag{82b}$$

$$X_{t,l,k} \geq \Im_1(t,l,k), \tag{82c}$$

$$Y_{t,l,k} \leq \Im_2(t,l,k), \tag{82d}$$

$$(40\text{i}), (81), \tag{82e}$$

which can be solved by CVX.

The proposed AO algorithm is outlined in Algorithm 1.

Algorithm 1 Alternating Optimization for Problem (40)

Initialize $\varsigma=0$, $\mathbf{w}$, $\boldsymbol{\Theta}$, $\mathbf{q}$, $\mathcal{U}$
repeat
  $\varsigma=\varsigma+1$
  if $\max\left\|\mathcal{U}_t^{(\varsigma)}-\mathcal{U}_t^{(\varsigma-1)}\right\|>\epsilon$ **then**
    Update $\mathcal{U}_t$, $\wp_{t,k}^{(\varsigma)}$ by solving (65)
  end if
  Update $b_{t,k}$
  Update $\delta_{t,k}^*$, by (44)
  Update $\mathbf{w}_t$, by (46)
  Update $\boldsymbol{\Theta}_t$, by (65)
  Update $\mathbf{q}_{t,r}$, by (82)
  Compute $\Upsilon_t^{(\varsigma)}$.
until $|\Upsilon_t^{(\varsigma)}-\Upsilon_t^{(\varsigma-1)}|\leq\epsilon$
return $\mathbf{w}^*$, $\boldsymbol{\Theta}^*$, $\mathbf{q}^*$, $\mathcal{U}^*$, Υ_t^*

Convergence Analysis: Due to the iterative nature of Algorithm 1, it is essential to verify its convergence to ensure the effectiveness of the proposed AO framework. Let $\left(\mathcal{U}^{(\varsigma)},\mathbf{w}^{(\varsigma)},\boldsymbol{\Theta}^{(\varsigma)},\mathbf{q}^{(\varsigma)}\right)$ denote the feasible solutions obtained at the ς-th iteration. The optimization process proceeds as $\cdots \rightarrow \left(\mathcal{U}^{(\varsigma+1)},\mathbf{w}^{(\varsigma)},\boldsymbol{\Theta}^{(\varsigma)},\mathbf{q}^{(\varsigma)}\right) \rightarrow \left(\mathcal{U}^{(\varsigma+1)},\mathbf{w}^{(\varsigma+1)},\boldsymbol{\Theta}^{(\varsigma)},\mathbf{q}^{(\varsigma)}\right) \rightarrow \left(\mathcal{U}^{(\varsigma+1)},\mathbf{w}^{(\varsigma+1)},\boldsymbol{\Theta}^{(\varsigma+1)},\mathbf{q}^{(\varsigma)}\right) \rightarrow \left(\mathcal{U}^{(\varsigma+1)},\mathbf{w}^{(\varsigma+1)},\boldsymbol{\Theta}^{(\varsigma+1)},\mathbf{q}^{(\varsigma+1)}\right) \rightarrow \ldots$. The subproblem (65), which is solved using DC programming relaxation for the binary user-RIS association variables, is optimized sequentially while keeping the remaining variables fixed. Consequently, the objective function exhibits a monotonic improvement behavior across iterations, which can be expressed as

$$\begin{aligned} & \Upsilon_t^{(\varsigma+1)}(\mathcal{U}^{(\varsigma+1)},\mathbf{w}^{(\varsigma)},\boldsymbol{\Theta}^{(\varsigma)},\mathbf{q}^{(\varsigma)}) \\ & \geq \Upsilon_t^{(\varsigma)}(\mathcal{U}^{(\varsigma)},\mathbf{w}^{(\varsigma)},\boldsymbol{\Theta}^{(\varsigma)},\mathbf{q}^{(\varsigma)}). \end{aligned} \tag{83}$$

Likewise, for problem (46), which is convex in $\mathbf{w}$ and solved as a maximization problem, the objective value Υ_t gradually

increases across iterations, i.e.,

$$\Upsilon_t^{(\varsigma+1)}(\mathcal{U}^{(\varsigma+1)}, \mathbf{w}^{(\varsigma+1)}, \mathbf{\Theta}^{(\varsigma)}, \mathbf{q}^{(\varsigma)}) \geq \Upsilon_t^{(\varsigma+1)}(\mathcal{U}^{(\varsigma+1)}, \mathbf{w}^{(\varsigma)}, \mathbf{\Theta}^{(\varsigma)}, \mathbf{q}^{(\varsigma)}). \quad (84)$$

The optimal $\mathbf{\Theta}$ is derived by solving problem (65), which maximizes the weighted sum-rate, and it satisfies:

$$\Upsilon_t^{(\varsigma+1)}(\mathcal{U}^{(\varsigma+1)}, \mathbf{w}^{(\varsigma+1)}, \mathbf{\Theta}^{(\varsigma+1)}, \mathbf{q}^{(\varsigma)}) \geq \Upsilon_t^{(\varsigma+1)}(\mathcal{U}^{(\varsigma+1)}, \mathbf{w}^{(\varsigma+1)}, \mathbf{\Theta}^{(\varsigma)}, \mathbf{q}^{(\varsigma)}). \quad (85)$$

Finally, $\mathbf{q}^{(\varsigma+1)}$ represents the optimal solution to the problem (82), and it can be expressed as

$$\Upsilon_t^{(\varsigma+1)}(\mathcal{U}^{(\varsigma+1)}, \mathbf{w}^{(\varsigma+1)}, \mathbf{\Theta}^{(\varsigma+1)}, \mathbf{q}^{(\varsigma+1)}) \geq \Upsilon_t^{(\varsigma+1)}(\mathcal{U}^{(\varsigma+1)}, \mathbf{w}^{(\varsigma+1)}, \mathbf{\Theta}^{(\varsigma+1)}, \mathbf{q}^{(\varsigma)}). \quad (86)$$

Thus, the objective function Υ_t exhibits a monotonic, increasing behavior across iterations. Since Υ_t is inherently bounded due to the power constraints, the proposed AO-based algorithm is guaranteed to converge to a stationary solution. The AO framework ensures convergence to a locally optimal solution that satisfies the Karush-Kuhn-Tucker (KKT) conditions.

Computational Complexity: This subsection summarizes the computational complexity of the Algorithm 1. In each iteration, three optimization subproblems are updated sequentially.

First, the beamforming update in (46) is formulated as a QCQP after applying the MCQT transformation. This block involves $LM(K+1)$ variables, and the associated matrix operations scale as $\mathcal{O}((LM(K+1))^3)$.

Second, the RIS phase shift and RIS-user association update in (65) jointly optimizes RN phase variables and KR association variables. The SCA/DC update requires matrix operations with complexity on the order of $\mathcal{O}((RN)^3 + (KR)^3)$.

Third, the UAV location update in (82) optimizes $2R$ position variables, and the resulting convex update has a computational order of $\mathcal{O}(R^3)$.

By combining the dominant terms of the three blocks, the overall complexity of one iteration can be expressed as $\mathcal{O}\big((LM(K+1))^3 + (RN)^3 + (KR)^3 + R^3\big)$.

V. SIMULATION RESULTS

This section presents the simulation outcomes to evaluate the performance of CF-ISAC system with URISs. In the considered setup, there are $L = 4$ distributed APs, $K = 4$ users, $R = 4$ RISs, and $F = 4$ SRs. The users and sensing target each have a single antenna, while both the APs and SRs are equipped with 4 antennas. Each RIS is composed of $N = 10$ passive reflecting elements. The maximum transmit power at each AP is limited to $P_{t,l}^{\max} = 1\,\text{W}$, and the noise power is set to $\sigma^2 = -110\,\text{dBm}$. The minimum SNR threshold for sensing are set at $\gamma_{th}^{sens} = 1$ dB. All APs, users, and SRs are uniformly distributed within a total area of 100 m × 100 m.

We implement the algorithms using MATLAB R2023b and solve the convex optimization problems with the SDPT3 solver. The iteration process is stopped when the improvement in the objective function between two consecutive steps becomes less than 10^{-3}. We evaluate the proposed algorithm by comparing it with three benchmark schemes, as follows:

- CF with fixed RISs: In this scheme, each RIS is installed at a fixed location, such as on a wall or a tall building.
- CF without URISs: In this scheme, we exclude the use of RIS-mounted UAVs.
- Collocated with URISs: In this scheme, a single AP is placed at the center of the area to serve all users. This AP is equipped with LM antennas and has a maximum transmit power of $LP_{t,l}^{\max}$.

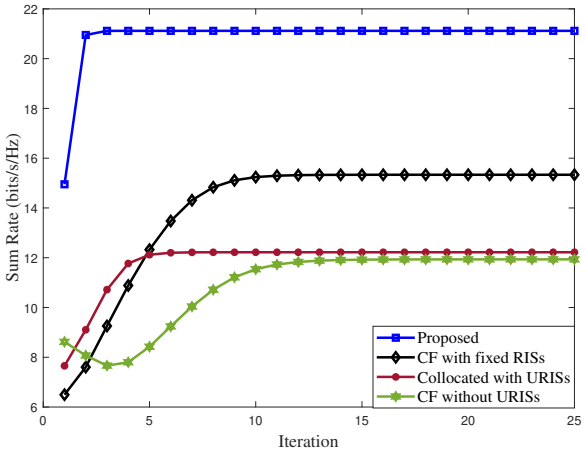

Fig. 3. Convergence behavior of Algorithm 1.

Fig. 3 shows the convergence behavior of Algorithm 1. Our proposed scheme achieves the highest sum rate of approximately 21.11 bits/s/Hz compared to other baseline schemes, and converges within just four iterations, demonstrating fast and efficient convergence. In comparison, CF with fixed RISs, Collocated with URISs, and CF without URISs schemes converge to lower sum rates of 15.33, 12.22, and 11.93 bits/s/Hz, respectively. This clearly highlights the effectiveness of our proposed algorithm in maximizing the sum rate. We note that the convergence speed may vary under certain conditions, such as very large optimization dimensions or highly time-varying UAV–RIS channels, which aligns with known behaviors of AO and block-coordinate methods.

Fig. 4 shows the impact of the number of RIS's elements on the sum rate of the users with respect to the association of the users. As the number of RIS's elements increases from 10 to 45, our proposed scheme consistently achieves the highest sum rate in both cases. Notably, when each user is allowed to associate with up to 4 RISs, the sum rate improves from 21.11 to 24.5 bits/s/Hz. In contrast, the 2 RISs association case shows a more modest improvement from 19 to 22.8 bits/s/Hz. This demonstrates that enabling users to be served with greater number of RISs enhances spatial diversity and system flexibility, leading to better spectral efficiency. Additionally, CF with fixed RISs and Collocated with URISs schemes follow similar trends, but their overall gains are significantly smaller, and the performance gap between the 2 RISs and 4 RISs settings is more modest. At $N = 10$ elements, the proposed scheme with maximum 4 RISs per

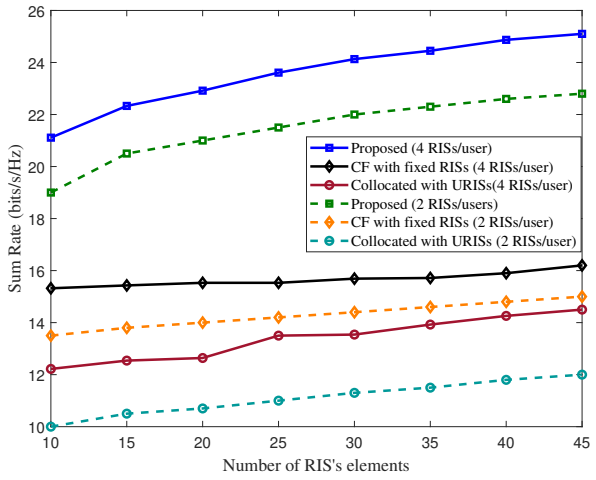

Fig. 4. The effect of number of RIS's elements on sum rate of users under different user-RIS associations.

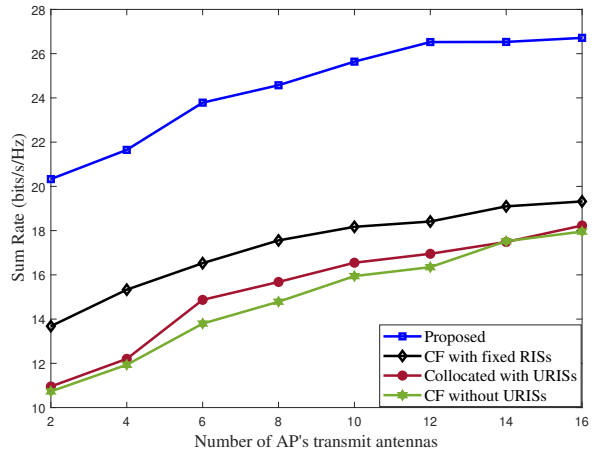

Fig. 5. The effect of number of AP's transmit antennas on sum rate of users.

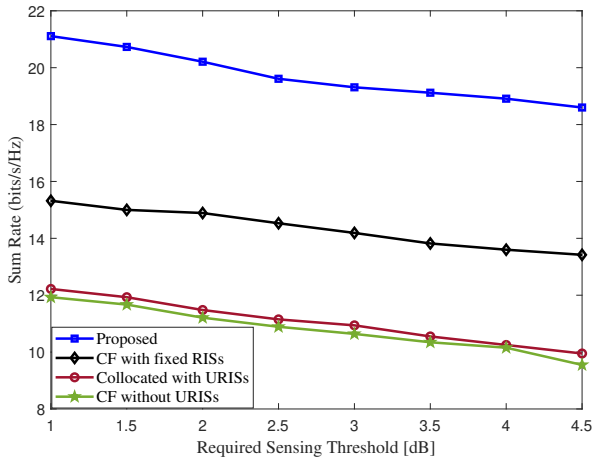

Fig. 6. The impact of sensing threshold on sum rate of users.

users outperforms CF with fixed RISs and Collocated with URISs by 37.7% and 72.8%, respectively.

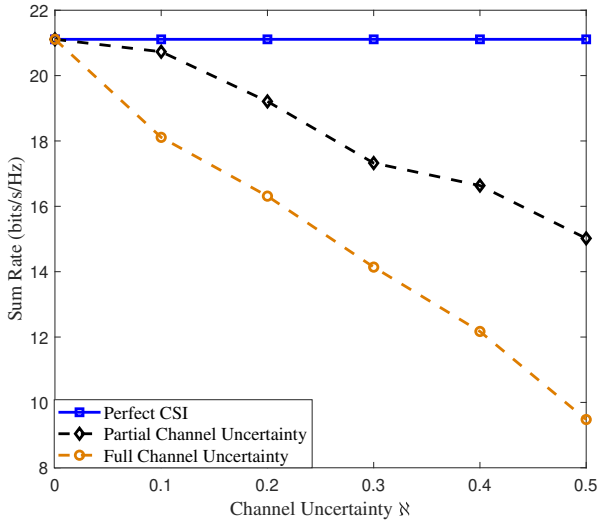

Fig. 7. The effect of channel uncertainty ℵ on sum rate of users.

Fig. 5 illustrates the impact of the number of AP's transmit antennas on the sum rate of users. At $M = 4$ antennas, the proposed scheme outperforms CF with fixed RISs, Collocated with URISs, and CF without URISs schemes by 32.2%, 48.7%, and 54.8%, respectively. This improvement is due to the fact that more antennas provide better spatial diversity and stronger beamforming capabilities, enabling the system to transmit signals more efficiently and reliably compared to the baseline schemes.

Fig. 6 illustrates the trade-off between communication performance and sensing requirement. It is clear that the weighted sum rate for all cases decreases as the sensing SNR threshold increases. This happens because a stricter sensing constraint requires more power for the sensing beamformer, leaving less power available to optimize the communication beamformers for maximizing the weighted sum rate. Besides, our proposed scheme considerably outperforms the CF-ISAC systems with fixed RISs and without URISs, thus confirming that the proposed scheme better balances the trade-off between sensing and communication, maintaining higher spectral efficiency even under stringent sensing constraints.

In passive RIS-assisted systems, accurate acquisition of the cascaded CSI is essential for efficient transceiver and RIS phase shift optimization. In practice, however, channel estimation errors and time-varying propagation conditions introduce uncertainty in the estimated CSI [45]. To examine the robustness of the proposed design under such imperfections, we adopt a bounded CSI error model for the cascaded AP–URIS–user channel. The imperfect channels are modeled as

$$\mathbf{G}_{t,l,r} = \hat{\mathbf{G}}_{t,l,r} + \Delta\mathbf{G}_{t,l,r}, \tag{87}$$

$$\mathbf{g}_{t,r,k} = \hat{\mathbf{g}}_{t,r,k} + \Delta\mathbf{g}_{t,r,k}, \tag{88}$$

where $\hat{\mathbf{G}}_{t,l,r}$ and $\hat{\mathbf{g}}_{t,r,k}$ denote the estimated CSI available at the central server, respectively. $\Delta\mathbf{G}_{t,l,r}$ and $\Delta\mathbf{g}_{t,r,k}$ represent the estimation errors, which satisfy the following conditions:

$$||\Delta \mathbf{G}_{t,l,r}||_F \leq \aleph ||\mathbf{G}_{t,l,r}||_F, \tag{89}$$

$$||\Delta \mathbf{g}_{t,r,k}||_2 \leq \aleph ||\mathbf{g}_{t,r,k}||_2, \tag{90}$$

where $\aleph \in [0, 1)$ denotes the level of CSI uncertainty.

We study two cases of channel uncertainty: partial and full. In the partial channel uncertainty, only the cascaded channel is considered uncertain, as described in (87) and (88). For the full channel uncertainty, it accounts for both the cascaded and direct channels, where the bounded error model is also applied to the AP-user direct link. As shown in Fig. 7, the achievable sum rate decreases as the uncertainty level $\aleph$ increases. Under perfect CSI, the proposed scheme achieves the highest sum rate, while performance degradation becomes more evident under the full channel uncertainty due to errors in both the cascaded and direct links. Nevertheless, the relative performance advantage of the proposed URIS-assisted CF ISAC system is largely preserved across all uncertainty levels, as the CSI errors affect the proposed and baseline schemes in a similar manner [21], [46].

VI. Conclusion

In this paper, we proposed an efficient AO framework for URISs assisted CF-ISAC system. Our approach jointly optimizes APs' transmit beamforming, RISs' phase shifts, RIS-user association, and URISs' locations to maximize the sum of achievable weighted sum rates within the whole ISAC period while satisfying radar sensing and UAVs' energy constraints. The original non-convex problem is decomposed and solved iteratively through tractable subproblems. Simulation results demonstrate significant performance improvements, showcasing the potential of our proposed approach for future RIS-mounted UAVs assisted CF-ISAC applications.

This work focused on a single sensing target for tractability. Extending the framework to multiple targets while accounting for inter-target interference, additional channel estimation overhead, and increased optimization complexity represents an important direction for future research. Future work will also focus on investigating dynamic URIS trajectories with user mobility, applying machine learning for adaptive optimization, and exploring sensing-communication trade-offs in more complex environments.

References

[1] Q. Xue, C. Ji, S. Ma, J. Guo, Y. Xu, Q. Chen, and W. Zhang, "A survey of beam management for mmWave and THz communications towards 6G," *IEEE Commun. Surv. Tutor.*, vol. 26, no. 3, pp. 1520–1559, 3rd Quart. 2024.

[2] S. Shakoor, Z. Kaleem, M. I. Baig, O. Chughtai, T. Q. Duong, and L. D. Nguyen, "Role of UAVs in public safety communications: Energy efficiency perspective," *IEEE Access*, vol. 7, pp. 140 665–140 679, Sep. 2019.

[3] Z. Wei, H. Qu, Y. Wang, X. Yuan, H. Wu, Y. Du, K. Han, N. Zhang, and Z. Feng, "Integrated sensing and communication signals toward 5G-A and 6G: A survey," *IEEE Internet Things J.*, vol. 10, no. 13, pp. 11 068–11 092, Jul. 2023.

[4] S. Lu, F. Liu, Y. Li, K. Zhang, H. Huang, J. Zou, X. Li, Y. Dong, F. Dong, J. Zhu *et al.*, "Integrated sensing and communications: Recent advances and ten open challenges," *IEEE Internet Things J.*, vol. 11, no. 11, pp. 19 094–19 120, Jun. 2024.

[5] J. M. Mateos-Ramos, C. Häger, M. F. Keskin, L. Le Magoarou, and H. Wymeersch, "Model-driven end-to-end learning for integrated sensing and communication," in *Proc. IEEE Int. Conf. Commun. (ICC)*, Rome, Italy, Oct. 2023, pp. 5695–5700.

[6] A. A. Salem, M. A. Albreem, K. Alnajjar, S. Abdallah, and M. Saad, "Integrated cooperative sensing and communication for RIS-enabled full-duplex cell-free MIMO systems," *IEEE Trans. Commun.*, vol. 73, no. 6, pp. 3804–3819, Nov. 2024.

[7] Z. Behdad, Ö. T. Demir, K. W. Sung, E. Björnson, and C. Cavdar, "Power allocation for joint communication and sensing in cell-free massive MIMO," in *Proc. IEEE GLOBECOM*, Rio de Janeiro, Brazil, Dec. 2022, pp. 4081–4086.

[8] K. Meng, C. Masouros, A. P. Petropulu, and L. Hanzo, "Cooperative ISAC networks: Performance analysis, scaling laws and optimization," *IEEE Trans. Wirel. Commun.*, vol. 24, no. 2, pp. 877–892, Feb. 2025.

[9] P. Gao, L. Lian, and J. Yu, "Cooperative ISAC with direct localization and rate-splitting multiple access communication: A pareto optimization framework," *IEEE J. Sel. Areas Commun.*, vol. 41, no. 5, pp. 1496–1515, May. 2023.

[10] H. Luo, R. Liu, M. Li, and Q. Liu, "RIS-aided integrated sensing and communication: Joint beamforming and reflection design," *IEEE Trans. Veh. Technol*, vol. 72, no. 7, pp. 9626–9630, Feb. 2023.

[11] M. Luan, B. Wang, Z. Chang, T. Hämäläinen, and F. Hu, "Robust beamforming design for RIS-aided integrated sensing and communication system," *IEEE Trans. Intell. Transp. Sys.*, vol. 24, no. 6, pp. 6227–6243, Jun. 2023.

[12] H. Zhao, F. Wu, W. Xia, Y. Zhang, Y. Ni, and H. Zhu, "Joint beamforming design for RIS-aided secure integrated sensing and communication systems," *IEEE Commun. Lett.*, vol. 27, no. 11, pp. 2943–2947, Nov. 2023.

[13] H. Luo, R. Liu, M. Li, Y. Liu, and Q. Liu, "Joint beamforming design for RIS-assisted integrated sensing and communication systems," *IEEE Trans. Veh. Technol.*, vol. 71, no. 12, pp. 13 393–13 397, Dec. 2022.

[14] D. Bao and R. Guo, "A dual function intelligent reflecting surface in integrated radar communication system," *IEEE Trans. Intell. Transp. Syst.*, vol. 26, no. 3, pp. 3471–3481, Jan. 2025.

[15] X. Yuan, Y. Hu, J. Zhang, and A. Schmeink, "Joint user scheduling and UAV trajectory design on completion time minimization for UAV-aided data collection," *IEEE Trans. Wireless Commun.*, vol. 22, no. 6, pp. 3884–3898, Jun. 2022.

[16] D. Tyrovolas, N. A. Mitsiou, T. G. Boufikos, P.-V. Mekikis, S. A. Tegos, P. D. Diamantoulakis, S. Ioannidis, C. K. Liaskos, and G. K. Karagiannidis, "Energy-aware trajectory optimization for UAV-mounted RIS and full-duplex relay," *IEEE Internet Things J.*, vol. 11, no. 13, pp. 24 259–24 272, Apr. 2024.

[17] Y. Song, Y. Qian, L. Chen, Z. Yan, F. Shu, and P. Zhu, "Joint beamforming and user association design in active RIS-aided cell-free URLLC system," in *16th IEEE WCSP*, Hefei, China, Oct. 2024, pp. 242–247.

[18] Q. Bie, Z. Liang, Y. Liu, Q. Wu, X. Zhao, and X. Y. Zhang, "User association for reconfigurable intelligent surfaces aided cell-free networks," *IEE Trans. Veh. Technol.*, vol. 72, no. 11, pp. 14 456–14 467, Oct. 2023.

[19] K. Chen, C. Qi, O. A. Dobre, and G. Y. Li, "Simultaneous beam training and target sensing in ISAC systems with RIS," *IEEE Trans. Wireless Commun.*, vol. 23, no. 4, pp. 2696–2710, Apr. 2024.

[20] Z. Liu, Y. Liu, S. Shen, Q. Wu, and Q. Shi, "Enhancing ISAC network throughput using beyond diagonal RIS," *IEEE Wirel. Commun.*, vol. 13, no. 6, pp. 1670–1674, Apr. 2024.

[21] X. Li, Q. Zhu, Y. Chen, C. Assi, and Y. Yuan, "Sensing for communication: RIS-assisted ISAC coordination gain enhancement with imperfect CSI," *IEEE Trans. Wireless Commun.*, vol. 24, no. 10, pp. 8145–8161, Oct. 2025.

[22] X. Zhu, J. Liu, L. Lu, T. Zhang, T. Qiu, C. Wang, and Y. Liu, "Enabling intelligent connectivity: A survey of secure ISAC in 6G networks," *IEEE Commun. Surv. Tutor.*, vol. 27, no. 2, pp. 748–781, Jul. 2025.

[23] U. Demirhan and A. Alkhateeb, "Cell-free ISAC MIMO systems: Joint sensing and communication beamforming," *IEEE Trans. Commun.*, vol. 73, no. 6, pp. 4454–4468, Jun. 2025.

[24] M. Elfiatoure, M. Mohammadi, H. Q. Ngo, and M. Matthaiou, "Cell-free massive MIMO for ISAC: Access point operation mode selection and power control," in *Proc. IEEE GLOBECOM*, Kuala Lumpur, Malaysia, Dec. 2023, pp. 104–109.

[25] Z. Behdad, Ö. T. Demir, K. W. Sung, E. Björnson, and C. Cavdar, "Multi-static target detection and power allocation for integrated sensing and communication in cell-free massive MIMO," *IEEE Trans. Wireless Commun.*, vol. 23, no. 9, pp. 11 580–11 596, Apr. 2024.

[26] Y. Fan, S. Wu, X. Bi, and G. Li, "Power allocation for cell-free massive MIMO ISAC systems with OTFS signal," *IEEE Internet Things J.*, vol. 12, no. 7, pp. 9314–9331, Apr. 2025.

[27] Z. Ren, J. Xu, L. Qiu, and D. W. K. Ng, "Secure cell-free integrated sensing and communication in the presence of information and sensing eavesdroppers," *IEEE J. Sel. Areas Commun.*, vol. 42, no. 11, pp. 3217–3231, Nov. 2024.

[28] S. Shakoor, Q. N. Le, E.-K. Hong, B. Canberk, and T. Q. Duong, "Integrated sensing and communications for reconfigurable intelligent surface-aided cell-free networks," *IEEE Commun. Lett.*, vol. 29, no. 6, pp. 1275–1279, Jun. 2025.

[29] X. Chen, X. Cao, L. Xie, and Y. He, "DRL-based joint trajectory planning and beamforming optimization in aerial RIS-assisted ISAC system," in *Proc. IEEE iWRFAT*, vol. 23, no. 9, Shenzhen, China, Jul. 2024, pp. 510–515.

[30] X. Song, D. Li, J. Tang, N. Zhao, Z. Yang, Z. Yin, and Z. Wu, "Enhancing cell-free network: Joint beamforming and location optimization via UAV-IRS," *IEE Trans. Veh. Technol.*, vol. 74, no. 1, pp. 1196–1208, Sep. 2025.

[31] W. Yang, Y. Wang, D. Wang, Y. He, and L. Li, "Secrecy-constrained UAV-mounted RIS-assisted ISAC networks: Position optimization and power beamforming," *Drones*, vol. 9, no. 1, p. 51, Jan. 2025.

[32] S. Liu, R. Liu, M. Li, Y. Liu, and Q. Liu, "Joint BS-RIS-user association and beamforming design for RIS-assisted cellular networks," *IEEE Trans. Veh. Technol.*, vol. 72, no. 5, pp. 6113–6128, May 2023.

[33] S. Rivetti, O. T. Demir, E. Bjornson, and M. Skoglund, "Clutter-aware target detection for ISAC in a millimeter-wave cell-free massive MIMO system," in *Proc. SPAWC*, Surrey, UK, Jul. 2025, pp. 1–5.

[34] S. Shakoor, Q. N. Le, L. D. Nguyen, K. Singh, O. A. Dobre, and T. Q. Duong, "Max-min fairness in active aerial reconfigurable intelligent surface-aided ISAC network," *IEEE Trans. Cogn. Commun. Netw.*, vol. 11, no. 5, pp. 2910–2922, Oct. 2025.

[35] H. Zheng and J. Yuan, "An integrated mission planning framework for sensor allocation and path planning of heterogeneous multi-UAV systems," *Sensors*, vol. 21, no. 10, p. 3557, May 2021.

[36] Q. Wu, Y. Zeng, and R. Zhang, "Joint trajectory and communication design for multi-UAV enabled wireless networks," *IEEE Trans. Wireless Commun.*, vol. 17, no. 3, pp. 2109–2121, Mar. 2018.

[37] Y. Zeng and R. Zhang, "Energy-efficient UAV communication with trajectory optimization," *IEEE Trans. Wireless Commun.*, vol. 16, no. 6, pp. 3747–3760, Mar. 2017.

[38] G. Zhou, C. Pan, H. Ren, P. Popovski, and A. L. Swindlehurst, "Channel estimation for RIS-aided multiuser millimeter-wave systems," *IEEE Trans. Signal Process.*, vol. 70, pp. 1478–1492, Mar. 2022.

[39] A. A. Nasir, "Joint users' secrecy rate and target's sensing SNR maximization for a secure cell-free ISAC system," *IEEE Commun. Letters*, vol. 28, no. 7, pp. 1549–1553, Jul. 2024.

[40] A. Bazzi and M. Chafii, "Low dynamic range for RIS-aided bistatic integrated sensing and communication," *IEEE J. Sel. Areas Commun.*, vol. 43, no. 3, pp. 912–927, Mar. 2025.

[41] L. Pucci, S. K. Dehkordi, P. Jung, E. Paolini, A. Giorgetti, and G. Caire, "Performance analysis of multistatic integrated sensing and communication in the near/far field," in *Proc. IEEE PIMRC*, Valencia, Spain, Sep. 2024.

[42] K. Shen and W. Yu, "Fractional programming for communication systems—Part I: Power control and beamforming," *IEEE Trans. Signal Process.*, vol. 66, no. 10, pp. 2616–2630, May 2018.

[43] C. Deng, X. Fang, and X. Wang, "Beamforming design and trajectory optimization for UAV-empowered adaptable integrated sensing and communication," *IEEE Trans. Wireless Commun.*, vol. 22, no. 11, pp. 8512–8526, Apr. 2023.

[44] B. Liu, Y. Wan, F. Zhou, Q. Wu, and R. Q. Hu, "Resource allocation and trajectory design for MISO UAV-assisted MEC networks," *IEEE Trans. Veh. Technol*, vol. 71, no. 5, pp. 4933–4948, Jan. 2022.

[45] P. R. Gomes, G. T. de Araujo, B. Sokal, A. L. de Almeida, B. Makki, and G. Fodor, "Channel estimation in RIS-assisted MIMO systems operating under imperfections," *IEEE Trans. Veh. Technol*, vol. 72, no. 11, pp. 14 200–14 213, May 2023.

[46] C. Jiang, C. Zhang, C. Huang, J. Ge, D. Niyato, and C. Yuen, "Ris-assisted ISAC systems for robust secure transmission with imperfect sense estimation," *IEEE Trans. Wireless Commun.*, vol. 24, no. 5, pp. 3979–3992, May 2025.